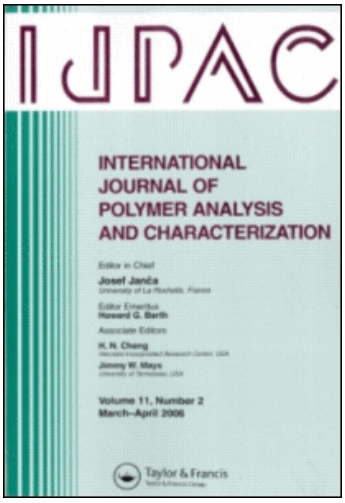


International Journal of Polymer Analysis and Characterization
Publication details, including instructions for authors and subscription information:
http://www.informaworld.com/smpp/title~content=t713646643

# Light Scattering Studies on Dilute Solutions of Semiflexible Polyelectrolytes

V. J. Sullivan[ab]; G. C. Berry
[a] Department of Chemistry, Carnegie Mellon University, Pittsburgh, PA [b] Hoechst-Celanese Corp., Summit, NJ

**To cite this Article** Sullivan, V. J. and Berry, G. C.(1995) 'Light Scattering Studies on Dilute Solutions of Semiflexible Polyelectrolytes', International Journal of Polymer Analysis and Characterization, 2: 1, 55 — 69
**To link to this Article: DOI:** 10.1080/10236669508233895
**URL:** http://dx.doi.org/10.1080/10236669508233895

*Int. J. Polymer Analysis & Characterization*
1995, Vol. 2, pp. 55–69
Reprints available directly from the publisher
Photocopying permitted by license only



# Light Scattering Studies on Dilute Solutions of Semiflexible Polyelectrolytes

V. J. SULLIVAN[a] and G. C. BERRY

*Department of Chemistry, Carnegie Mellon University, Pittsburgh, PA 15213*

*(Received September 26, 1994; revised December 5, 1994)*

Poly(1,4-phenylene-2,6-*cis*-benzobisoxazole) and poly(2,5-benzoxazole) represent examples of semiflexible chains, forming polyelectrolytes in solution in protic acids. Dilute solutions of these have been studied by static and dynamic light scattering and viscometry. Solutions have been prepared in acidic solvents over a wide range of ionic strength, and hence of Debye electrostatic screening length $\kappa^{-1}$. The data reveal electrostatic interactions among the protonated chains through a thermodynamic segment diameter $d_T$ that depends markedly on $\kappa^{-1}$. The analysis suggests that the electrostatic component $d_e$ to $d_T$ must be large enough to offset a neutral component $d_n$ in $d_T$, providing the mechanism for dissolution of the charged chains. The persistence length $\rho \approx 40$ nm for poly(1,4-phenylene-2,6-*cis*-benzobisoxazole), is essentially independent of $\kappa^{-1}$. Thus, for this chain the electrostatic component $\rho_e$ to $\rho$ must be small in comparison with the neutral component $\rho_n$ to $\rho$. This appears to be in reasonable accord with estimates of $\rho_n$ based on conformational analyses, and $\rho_e$ using an electrostatic model. By contrast, $\rho$ is found to depend markedly on $\kappa^{-1}$ for poly(2,5-benzoxazole), with $\rho$ much larger than $\rho_n$ for all of the systems studied. The observed $\kappa\rho$ vary from 20 to 50 with $\kappa^{-1}$ increasing from 0.8 to 8 nm for poly(2,5-benzoxazole). Thus, it may be considered to be a wormlike semiflexible chain in solvents with low $\kappa^{-1}$ (high ionic strength), and rodlike in solvents with larger $\kappa^{-1}$. By comparison, values of $\kappa\rho$ calculated with an electrostatic model based on a charged wormlike cylinder are about ten-fold smaller. The discrepancy is attributed to the failure of the model to account for the discrete rotational states available to the poly(2,5-benzoxazole) chain.

KEY WORDS Poly(2,5-benzoxazole), (1,4-phenylene-2,6-*cis*-benzobisoxazole), polyelectrolyte, semiflexible, wormlike, static light scattering, dynamic light scattering



## INTRODUCTION

The semiflexible chains poly(1,4-phenylene-2,6-*cis*-benzobisoxazole), *cis*-PBO, and poly(2,5-benzoxazole), *ab*-PBO, are each soluble only in reactive solvents, such as strong protic acids. In the latter, the chains are protonated by the acid to form a polycation [1–4]:

$$P + nRH \rightleftarrows P(H^+)_n + nR^-$$

where $P$ represents the polymer and $RH$ the acid solvent. Thus, electrostatic interactions may become important in determining the conformation of the semiflexible chain and the

Correspondence: Prof. G. C. Berry, Department of Chemistry, 4400 Fifth Avenue, Carnegie Mellon University, Pittsburgh, PA 15213

a) Present address: Hoechst-Celanese Corp., Summit, NJ 07901.

Presented at the 7th International Symposium on Polymer Analysis and Characterization, Les Diablerets, Switzerland, May 24–26, 1994.

interactions among the chain [5–19]. In addition, protonation may change the conformation of the repeat unit, with further effect on the overall chain conformation [15–17]. As may be seen in Figure 1, in the absence of electrostatic effects, the conformation of *cis*-PBO is expected to be more extended than that of *ab*-PBO owing to the nature of the chain structure [15–18]. Thus, the persistence lengths $\rho_n$ calculated for the neutral *cis*-PBO and *ab*-PBO chains differ significantly, with estimates being in the range 25 ~ 80 nm for *cis*-PBO[15–17] based on conformational models of varying sophistication, and ~ 5nm for *ab*-PBO assuming free rotation about the single bond between repeat units [18]. Both polymers will form an ordered (nematic) phase in concentrated solutions, with significantly higher concentration being required for *ab*-PBO than for *cis*-PBO of equivalent molecular weight in a solvent such as methane sulfonic acid [3,18,19].

In this study, light scattering and intrinsic viscosity measurements on dilute solutions are used to characterize the persistence length and intermolecular interactions for the *ab*-PBO and *cis*-PBO chains in solution in protic acids, in which the chains are highly protonated [1–4]. Solvents spanning a range of ionic strength have been used to study the effects of ionic strength on these parameters. The results will be compared with theoretical relations available in the literature [5–13]. Owing to substantial difficulties encountered with intermolecular association if the samples are fractionated with respect to chain length, this study has been conducted with the materials as polymerized, to permit a reasonable estimate of the effects of molecular weight distribution on the observed parameters. Principal conclusions of this study will be that electrostatic interactions play a dominant role in intermolecular interactions with both *ab*-PBO and *cis*-PBO in solvents with low ionic strength, whereas the radius of gyration of *ab*-PBO, but not that of *cis*-PBO, increases sharply as the ionic strength is decreased. Comparisons will be made with available theoretical predictions.

The notation ABPBO has been used to refer to poly(2,5-benzoxazole) in place of the equally unconventional notation *ab*-PBO used here, e.g., see reference 18 and citations

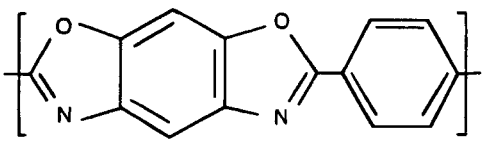


**Poly(1,4-phenylene-2,6-*cis*-benzobisoxazole), PPBO**

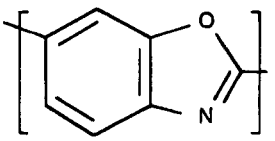


**Poly(2,5-benzoxazole), PBO**

FIGURE 1 Schematic drawings of the repeat units of the *cis*-PBO and *ab*-PBO polymers.

therein. The authors could devise no simpler notation since PBO has been used for some time to denote poly(1,4-phenylene-2,6-*cis*-benzobisoxazole).

## EXPERIMENTAL

### Materials

Both the *cis*-PBO and the *ab*-PBO samples used here were obtained from the Dow Chemical Co. through the courtesy of Dr. W.-F. Hwang. The general methods of polymerization have been discussed elsewhere [18]. The samples were received as dry powders, precipitated and washed free of contaminants from the polymerization solution. The samples were placed under vacuum (~ $10^{-4}$ torr) at 60°C for ~4 weeks, and heated to 100°C at ~$10^{-5}$ torr for at least 24 h immediately prior to use.

Methane sulfonic acid, MSA, and trifluoromethane sulfonic acid, FMSA, were received from Pennwalt Co. and 3M Co., respectively. Both solvents were distilled under an inert atmosphere before use (MSA under reduced pressure), and stored under dry conditions under nitrogen. Recent studies on MSA have shown that the distillation process used here may leave residual water, thereby enhancing the ionic strength of the solvent [20]. The ionic strength I of solutions studied in FMSA was varied by addition of lithium trifluoromethane sulfonate, obtained from Aldrich Chemical Co. The salt was placed under vacuum (~$10^{-5}$ torr) and heated with a flame just prior to use. The mixed solvent systems is designated by reference to the molarity of the lithium salt added, e.g., FMSA + 0.1M denotes FMSA with 0.1 molar added salt.

The ionic strength of the solvents used was deduced from measurements of the conductivity at 1000 Hz using a sealed cell fitted with platinum electrodes, following procedures described elsewhere, see below [3,21].



### Dilute Solution Characterization

Viscometry measurements were carried out under nitrogen using Ubbelohde viscometers. A bath with temperature fluctuations of less than ±0.01°C was used. Solutions in MSA were filtered through a 1 μm Zitex Teflon™ filter attached to the syringe used to deliver weighted amounts of solution (or solvent) to the viscometer. Since the filtration assembly was not inert to FMSA, a glass frit (average pore size 25 μm) was installed in the viscometers to filter the solution entering the capillary. Viscometers were chosen so that solvent flow times $t_s$ exceeded 200 seconds. Flow times were reproducible to ± 0.02%.

Light scattering experiments and measurements of refractive index increment dn/dc were carried out using instruments described elsewhere [2]. Solutions in MSA were filtered into light scattering cells through 1 micron Teflon™ filters as with viscometry measurements. FMSA solutions were filtered through glass frits of 1 micron average pore size. The samples were filtered into Danliker-Kraut type light scattering cells [2], then degassed and sealed on a vacuum line. Cells were centrifuged for 24 hours at 7000 rpm in a swinging bucket rotor.

## RESULTS

Specific conductances $K_{sp}$ of 0.0032 and 0.00022 ohm$^{-1}$cm$^{-1}$ were found for the samples of MSA and FMSA used here. For the univalent species of interest here, $K_{sp} = \Sigma\Lambda_i m_i$, with $m_i$ the molar concentration of species $i$, and the ionic strength $I_o = \Sigma m_i/2$ is related to $K_{sp}$ by

$$I_o = K_{sp}/\Lambda^-\{1 + \Lambda^+/\Lambda^-\} \quad (1)$$

Following procedures discussed elsewhere [3], $I_o$ was calculated from the observed $K_{sp}$ for MSA and FMSA on the assumption that the ratio $\Lambda^+/\Lambda^-$ of the ionic conductances of the cations ($RSO_3H_2^+$) and anions ($RSO_3^-$) produced on self-protonation of the solvent is equal to 1.45, as is the case for several sulfonic acids [21], and that $\Lambda^- = 75$ ohm$^{-1}$cm$^2$ for MSA [3,21] may also be used for FMSA (i.e., $I_o$/mol mL$^{-1} \approx 0.0054K_{sp}$/ohm$^{-1}$cm$^{-1}$). Since $I_o$ is small for FMSA ($\approx 2 \times 10^{-6}$ mol/mL), the ionic strength of the solvent containing 0.1M salt was calculated from the salt concentration. Values of the Debye screening length $\kappa^{-1} = (8\pi N_A L_B I_o)^{-1/2}$ are given in Table I, where $L_B = e^2/\epsilon kT$ is the Bjerrum length with $\epsilon$ the dielectric strength ($L_B$/nm $\approx 57/\epsilon$ at 25°C, or $L_B \approx 0.9$ nm for the solvents used here). For solutions in FMSA, the value of $\kappa^{-1}$ at infinite dilution is entered, since the value of $I_o$ increases significantly with increasing polymer concentration owing to the small value of $I_o$ of FMSA. Thus, $I_o = (I_o)^o + \nu_p m_p/2$, with $(I_o)^o$ the ionic strength at infinite dilution, $m_p$ the molar concentration (mol/mL) of polymer repeat units, and $\nu_p$ the degree of protonation of the polymeric repeat unit. Measurements of $K_{sp}$ for *cis*-PBO in FMSA give $\nu_p \approx 3$, in accord with estimates of the degree of protonation of *cis*-PBO [1].

Values of the specific viscosity $\eta_{sp} = (\eta - \eta_s)/\eta_s$ were determined over a range of polymer concentration c, with $\eta_{sp} < 1.8$ ($\eta$ and $\eta_s$ being the viscosities of solution and solvent, respectively). Data for concentrations with $\eta_{sp} > 0.2$ appear to follow the usual behavior, with [22]

$$\eta_{sp}/c = [\eta] + k'[\eta]^2 c + \ldots \quad (2a)$$

TABLE I

Parameters Determined for Two Semiflexible Polyelectrolytes in Solvents with Different Electrostatic Screening Length

| Polymer[a] | Solvent[a] | $\kappa^{-1}$[b] (nm) | $[\eta]$ (ml/g) | $M_w$ ×10$^{-4}$ | $M_w\delta^2$ ×10$^{-4}$ | $A_{2,LS}M_w$ (mL/g) | $R_{G,LS}$ (nm) | $R_{H,LS}$ (nm) |
|---|---|---|---|---|---|---|---|---|
| *cis*-PBO | FMSA | 7.9 | 2300 | 5.4[c] | 0.11 | 8100[c] | 84 | 22 |
| *cis*-PBO | MSA | 2.1 | 1300 | 5.7 | 0.11 | 1700 | 70 | 26 |
| *cis*-PBO | FMSA + 0.1M | 0.8 | 1700 | 5.4 | 0.11 | 970 | 62 | 23 |
| *ab*-PBO | FMSA | 7.9 | — | 6.95[c] | <0.04[d] | 7350 | 155 | — |
| *ab*-PBO | MSA | 2.1 | 1400 | 6.95 | 0.067 | 1950 | 64 | — |
| *ab*-PBO | FMSA + 0.1M | 0.8 | 1300 | 6.95 | <0.04[d] | 1200 | 54 | 20 |

a) *cis*-PBO = poly(1,4-phenylene-2.6-*cis*-benzobisoxazole); *ab*-PBO = poly(2,5-benzoxazole); MSA = methane sulfonic acid; FMSA = trifluoromethane sulfonic acid; FMSA + 0.1M = trifluoromethane sulfonic acid with 0.1M lithium trifluoromethane sulfonate.

b) The Debye electrostatic screening length, see text.

c) Determined by extrapolation assuming that $M_w$ is as obtained with the solvent containing 0.1M salt, see text.

d) An upper bound, the depolarized scattering $R_{Hv}$ was too small to be measured.

$$\ln(1+\eta_{sp})/c = [\eta] - \left(\frac{1}{2} - k'\right)[\eta]^2 c + \ldots \tag{2b}$$

where $k'$ is close to 1/3. The values of $[\eta]$ reported in Table I were obtained by extrapolation of $\eta_{sp}/c$ and $[\ln(\eta/\eta_s)]/c$ to infinite dilution, following standard practice. The behavior was abnormal in some cases for smaller $\eta_{sp}$, with $\eta_{sp}/c$ tending to increase with decreasing c, with this effect being most pronounced for solutions in FMSA. Data from that regime were not employed here. The data on $[\eta]$ obtained here for solutions in MSA and FMSA + 0.1M for *cis*-PBO and *ab*-PBO are similar to data reported in references 17 and 18, respectively, though $[\eta]$ obtained here is about 30% larger than that in reference 18 (the latter descripancy may be due in part to differences in dn/dc used to estimate $M_w$ from light scattering data, see below).

Light scattering results are analyzed according to the model for anisotropic scatterers [2,22–27]. This model provides equations for the dependence of vertical and horizontal components of light scattered with vertically polarized incident light, denoted $R_{Vv}(q)$ and $R_{Hv}(q)$, respectively, on the modulus $q = (4\pi n_s/\lambda)\sin(\vartheta/2)$ of scattering angle vector, where $n_s$ is the refractive index of the sample, $\lambda$ is the wavelength of light, and $\vartheta$ is the angle between the incident and scattered beams; notation for the dependence on c is suppressed for convenience). The polarized scattering $R_{Vv}(0)$ extrapolated to zero scattering angle provides information on the molecular weight M and the second virial coefficient $A_2$ [2,22–25]:

$$\left(\frac{Kc}{R_{Vv}(0)}\right)^{1/2} = \left(\frac{1}{M(1+4\delta^2/5)}\right)^{1/2}\left\{1 + \left(\frac{1-\delta^2/10}{1+4\delta^2/5}\right)A_2 Mc + \ldots\right\} \tag{3}$$

where $K = (2\pi^2/N_A\lambda^4)[n_o(\mathrm{dn/dc})]^2$, $n_o$ is the solvent refractive index, $N_A$ is Avogadro's number and $\delta$ the molecular anisotropy of the chain. The latter is a function of the chain conformation and the intrinsic anisotropy $\delta_o$ of the scattering elements making up the chain [2,23–25], see below.

Measurements of dn/dc gave 0.474 and 0.369 mL/g for *cis*-PBO and *ab*-PBO in MSA, respectively, and 0.629 and 0.541 mL/g for *cis*-PBO and *ab*-PBO in FMSA, respectively. Further, the latter values were also obtained for solutions in FMSA + 0.1M, indicating that the salt is essentially isorefractive with FMSA, simplifying the analysis of light scattering data [24–25]. Similar values dn/dc has been reported for MSA solutions of *cis*-PBO [17] and *ab*-PBO [18] (assuming that the units have been erroneously reported as dL/g instead of mL/g in the latter case).

When extrapolated to infinite dilution (denoted by a super zero), the angular dependence of the scattering provides a measure of the root-mean-square radius of gyration $R_G$ [22–25]:

$$\left(\frac{Kc}{R_{Vv}(q)}\right)^{o} = \frac{1}{M(1+4\delta^2/5)}\left\{1 + \frac{1}{3}(R_{G,V}q)^2 + \ldots\right\} \tag{4}$$

with $R_{G,V}^2 = J(\delta)R_G^2$, where

$$J(\delta) = \frac{j(\delta)}{1+4\delta^2/5} = \frac{1 - 4f_1\delta/5 + 4(f_2\delta)^2/7}{1+4\delta^2/5} \tag{5}$$

is unity for $\delta = 0$, and 3/7 for $\delta = 1$. The functions $f_1$ and $f_2$ tend to unity as $\delta/\delta_o$ tends to unity, and decrease approximately as ρ/L for large $L/\rho$ (coil) [23–25]. Consequently, $f_1$ and $f_2$ may be approximated as unity for practical purposes, since the effect of molecular anisotropy on $(Kc/R_{Vv}(q))^o$ is negligible for small $\delta/\delta_o$. The functions $Kc/R_{Vv}(q)$ vs q were found to be essentially linear and parallel over the concentration range studied. Plots of $[Kc/R_{Vv}(q)]_o]_o$ versus $\sin^2(\vartheta/2)$ for solutions of *cis*-PBO and *ab*-PBO in the three solvent systems studied are given in Figure 2. The extrapolated $[Kc/R_{Vv}(0)]$ are given as a function of concentration in Figure 3.

The depolarized scattering $R_{Hv}(0)$ extrapolated to zero scattering angle depends on the molecular weight $M$, the anisotropy δ, and the second virial coefficient $A_2$ [25,26]:

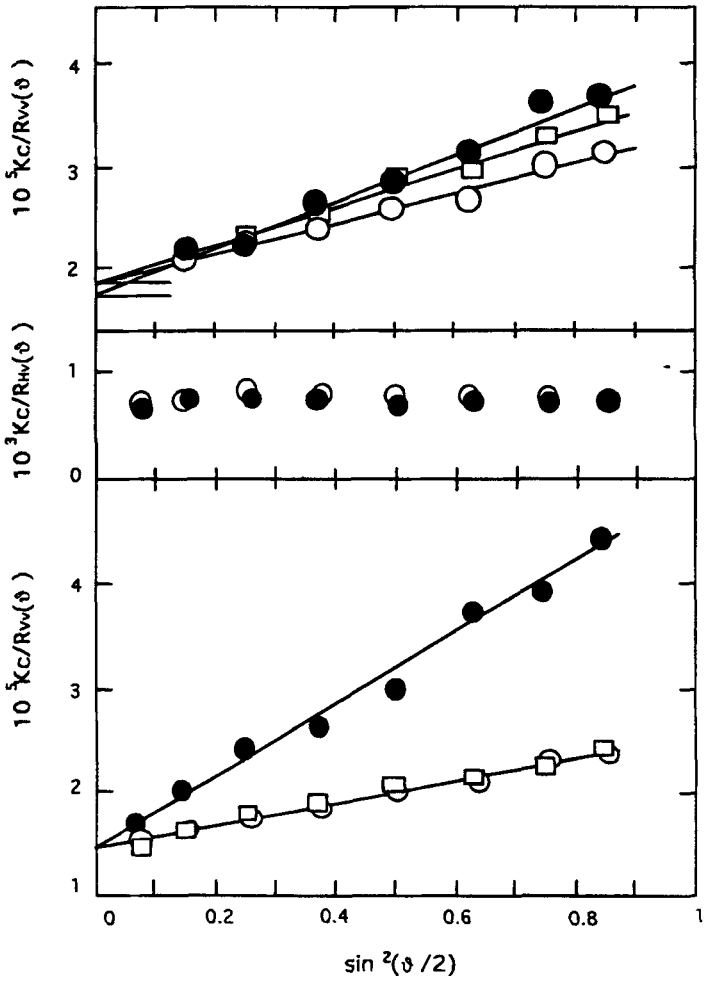


FIGURE 2 Upper: The angular dependence of $(Kc/R_{Vv}(\vartheta))$ for solutions of *cis*-PBO.
Middle: The angular dependence of $(Kc/R_{Hv}(\vartheta))$ for solutions of *cis*-PBO.
Lower: The angular dependence of $(Kc/R_{Vv}(\vartheta))$ for solutions of *ab*-PBO.
In each case, the symbols designate the solvent: Squares, methane sulfonic acid; Circles, trifloromethane sulfonic acid—without (filled) or with 0.1M lithium trifluoromethane sulfonate (unfilled).

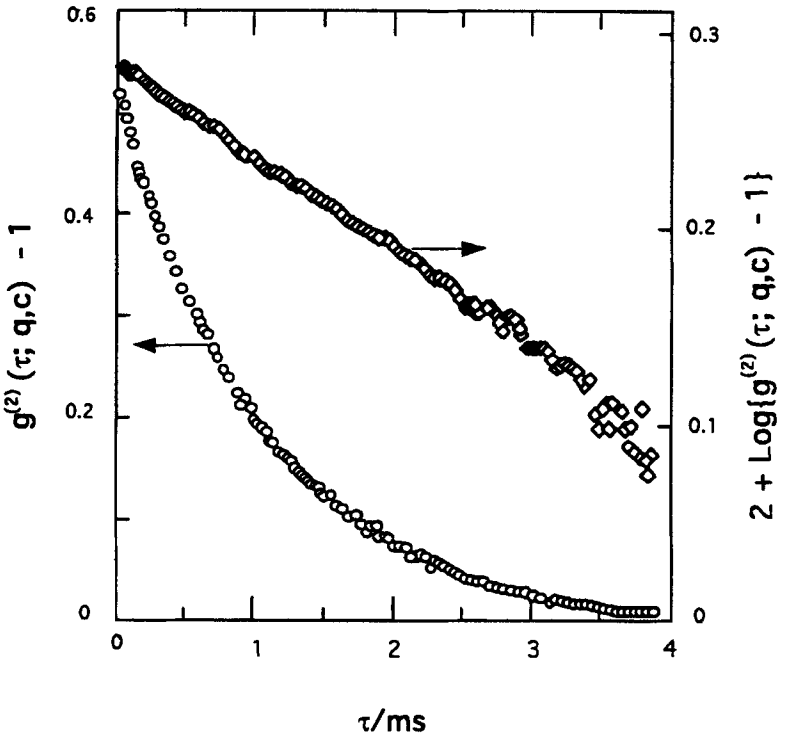


FIGURE 3 Upper: The concentration dependence of $(Kc/R_{Vv}(0))^{1/2}$ for solutions of *cis*-PBO.
Middle: The concentration dependence of $Kc/R_{Hv}(0)$ for solutions of *cis*-PBO.
Lower: The concentration dependence of $(Kc/R_{Vv}(0))^{1/2}$ *ab*-PBO (symbols as in Figure 2).
In each case, the symbols designate the solvent as in Figure 2.

$$\left(\frac{Kc}{R_{Hv}(0)}\right) = \frac{5}{3M\delta^2}\{1 - A_2Mc/4 + \ldots\} \tag{6}$$

or $Kc/R_{Hv}(q)\ \Omega\ [Kc/R_{Hv}(q)]^\circ = 5/3M\delta^2$ for typical values of $A_2$. Further (for $\delta \neq 0$) [23–25],

$$\left(\frac{Kc}{R_{Hv}(q)}\right)^\circ = \frac{5}{3\delta^2 M}\left\{1 + \frac{3}{7}(R_{G,H}q)^2 + \ldots\right\} \tag{7}$$

with $R^2_{G,H} = f_3^2 R_G^2$, where $f_3$ is similar in form to $f_1$ and $f_2$ [3–25], see below. Thus, $R^2_{G,H} = R^2_{G,V}/J(\delta) = R_G^2$ in the limit of a rodlike chain, but $R^2_{G,H} < R^2_{G,V} = R_G^2$ in the limit of a flexible chain. Values of $[Kc/R_{Hv}(q)]^\circ$ versus $sin^2(\vartheta/2)$ are given in Figure 2 for solutions of *cis*-PBO in the three solvent systems studied, and the extrapolated $[Kc/R_{Hv}(0)]$ are given as a function of concentration in Figure 3. Comparison of the reduced intensities extrapolated to zero angle and infinite dilution provides a measure of $\delta$:

$$\left(\frac{R_{Hv}(0)/c}{R_{Vv}(0)/c}\right)^\circ = \frac{3\delta^2}{5 + 4\delta^2} \tag{8}$$

Since the samples are heterodisperse, appropriate averages must be used for the derived parameters. Thus, from the polarized scattering [2,23–25,29,30],

$$(M_V)_{LS} = \Sigma w_v M_v (1 + 4\delta^2/5)_v = M_w + 4(\delta^2 M_H)_{LS}/5 \tag{9}$$

$$(R^2_{G,V})_{LS} = (M_V)^{-1}_{LS} \Sigma w_v M_v (j(\delta) R^2_G)_v \tag{10}$$

$$A_{2,LS} = (M_w^{-2} \Sigma \Sigma w_v M_v w_\mu M_\mu (A_2)_{v\mu} \tag{11}$$

The parameters from the depolarized scattering become

$$(\delta^2 M_H)_{LS} = \Sigma w_v (\delta^2 M)_v \tag{12}$$

$$(R^2_{G,H})_{LS} = \frac{\Sigma w_v M_v (f_3^2 \delta^2 R^2_G)_v}{\Sigma w_v (\delta^2 M)_v} \tag{13}$$

Results obtained by analysis of the static light scattering data are given in Table I. The data on $(R^2_{G,V})_{LS}$ and $A_{2,LS}M_w$ obtained in solutions of *cis*-PBO in MSA and FMSA + 0.1M are similar to reports in reference 17 for solutions of similar ionic strength (e.g., $(R^2_{G,V})_{LS}$ is about 25% larger than the value estimated from Figure 13 in reference 17 for solutions in MSA), but the data on $\delta$ for these systems are somewhat smaller than values reported in reference 17. Values of $A_{2,LS}M_w$ obtained in solutions of *ab*-PBO in MSA and FMSA + 0.1M are about two-fold smaller than reported in reference 18 for solutions in MSA (note that the estimate for $A_{2,LS}M_w$ does not depend on dn/dc).

Dynamic light scattering measurements were carried out to give the intensity auto-correlation function $g^{(2)}(\tau;q,c)$ as a function of scattering angle $q$ and correlation time $\tau$ [24,25,27]. Typical correlation functions are given in Figure 4. Nonexponential behavior was seen in all cases. With a cumulant analysis [25,27],

$$\ln[g^{(2)}(\tau;q,c) - 1]^{1/2} = -K_1(q,c)\tau + \frac{1}{2!}K_2(q,c)\tau^2 + \ldots \tag{14}$$

A nonlinear least-squares analysis was used to determine $K_1(q,c)$ and $K_2(q,c)$. The ratio $K_2/K_1^2$ provides a measure of the heterodispersity of the polymeric solute in the absence of contributions to $g^{(2)}(\tau; q,c)$ from rotational or internal modes of motion [25,27]. The ratio $|K_2/K_1^2|$ was small < 0.1 for most of the data obtained in FMSA or FMSA + 0.1M, but tended to be larger with solutions of *cis*-PBO in MSA. This may reflect some tendency for association of *cis*-PBO in MSA. A systematic dependence of the measured $K_1(q,c)/q^2$ on angle for *ab*-PBO/MSA, provides additional evidence for some association. In the limit of zero scattering angle, $D_M(c) = K_1(q,c)/q^2$ where $D_M(c)$ is the mutual diffusion coefficient. Values of $\eta_s D_M(c)$ are shown as a function of c in Figure 5. The extrapolation follows the usual form:

$$D_M(c) = D_T\{1 + (k_1 A_2 M - k_2[\eta])c + \ldots\} \tag{15}$$

where $D_T$ is the translational diffusion constant and $k_1$ and $k_2$ are constants of order unity [24,25]. Data are conveniently represented as a hydrodynamic radius $R_H = kT/6\pi\eta_s D_T$ to remove the effects of the solvent viscosity $\eta_s$ (values of 10.5, 3.12 and 2.81 cp were used for $\eta_s$ for MSA, FMSA + 0.1M, and FMSA, respectively). Since the samples are het-

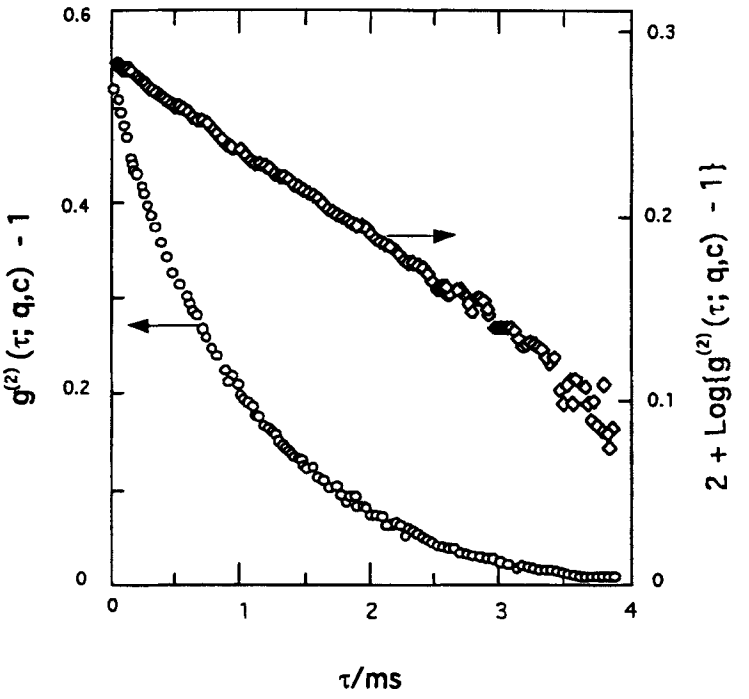


FIGURE 4 A typical photon count autocorrelation function $g^{(2)}(\tau;q,c)$ as a function of the correlation time $\tau$ (*ab*-PBO in FMSA + 0.1M, c = 0.58 g/L, $\vartheta = 45°$).

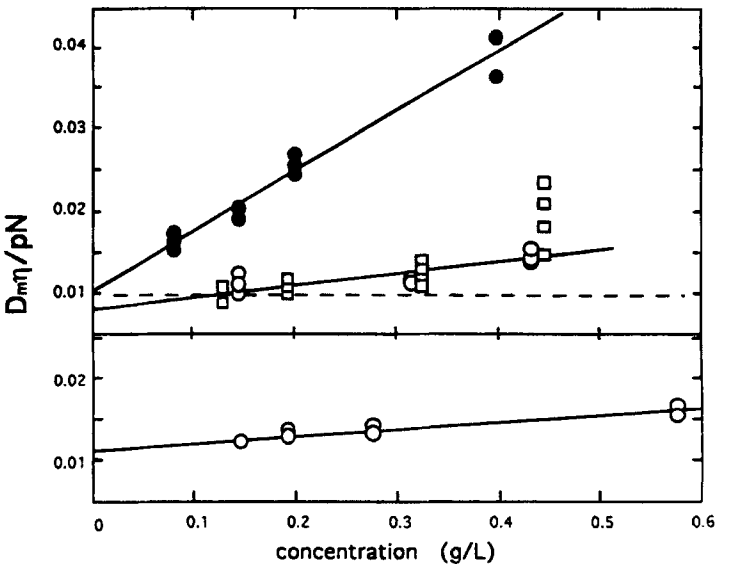


FIGURE 5 The concentration dependence of the reduced mutual diffusion constant $\eta_s D_m$ for solutions of *cis*-PBO (upper) and *ab*-PBO (lower). In each case, the symbols designate the solvent as in Figure 2.

erodisperse, an appropriate average must be used for the derived parameters [24,25,27],

$$R_{H,LS} = M_W/\Sigma w_v M_v (R_H^{-1})_v \tag{16}$$

Values of $R_{H,LS}$ are given in Table I.

## DISCUSSION

### The wormlike chain model

Since the wormlike chain model [22,28] will be used for the analysis of the characterization data, it is convenient to present all of the relations to be used in the following paragraphs, before turning to their application. With this model, the chain with molecular weight $M$ is characterized by a contour length $L$ and persistence length $\rho$, presumed to be independent of $L$. The mass per unit length $M_L = M/L$ is also presumed to be a constant; $M_L$ is equal to 183 $nm^{-1}$ and 203 $nm^{-1}$ for *cis*-PBO and *ab*-PBO, respectively. Interactions among chain segments are characterized by a thermodynamic diameter $d_T$ of a chain segment and certain hydrodynamic properties are characterized by a hydrodynamic diameter $\mathbf{d_H}$ of a chain segment. The latter is expected to be near the geometric diameter $d_G$ of a chain segment, but $d_T$ reduces to zero under Flory theta conditions ($A_2 = 0$), and may exceed $d_G$ for a charged chain, see below. Exact expressions [22] for $R^2_G$ and $R_H$ for the wormlike chain model may be represented by the simple relations [29,30]

$$R_G^2 \approx (L^2/12)(1 + L/4\rho)^{-1} \tag{17}$$

$$R_H \approx (L/2)\{(27L/16\rho) + [2(L/d_h)^{0.2}/f(L/d_h)]^2\}^{-1/2} \tag{18}$$

where $f(L/d_h) = 2(L/dh)^{0.2}/\ln(3L/2d_h)$ is approximately unity for the range of $L/d_h$ of interest here. For the wormlike chain model [23,24],

$$(\delta/\delta_o)^2 = (2\rho/3L)\{1 - (\rho/3L)[1 - \exp(-3L/\rho)]\} \approx (1 + 3L/2\rho)^{-1} \tag{19}$$

Consequently, the effects of optical anisotropy on $Kc/R_{Vv}(0)$ are expected to become negligible as $L/\rho$ exceeds about unity and the conformation becomes coil-like.

The second virial coefficient of a wormlike chain may be expressed in the form [22,25,31]

$$A_2 = A_2^{(R)} a(L/\rho, d_T/\rho, z) \tag{20}$$

$$A_2^{(R)} = (\pi N_A/4M_L^2)\, d_T \tag{21}$$

$$z = (3d_T/16\rho)(3L/\pi\rho)^{1/2} \tag{22}$$

$$a(L/\rho, d_T/\rho, z) \approx \{1 + 2.865Q(L/\rho, d_T/\rho)z/\alpha_o^3\}^{-1} \tag{23}$$

$$\alpha_o^2 = \{1 + 7.542\hat{z} + 11.06\hat{z}^2\}^{0.1772} \tag{24}$$

where $\hat{z} = A(L/\rho)z$, with $A(L/\rho)$ and $Q(L/\rho,d_T/\rho)$ known functions [22,25,28,31]. Both $A(L/\rho)$ and $Q(L/\rho,d_T/\rho)$ are unity for large $L/\rho$ (coil); $A(L/\rho)$ decreases to zero for small $L/\rho$ (an approximate analytical form is available [30]), but the behavior for $Q(L/\rho, d_T/\rho)$ is more complex, with $Q(L/\rho,d_T/\rho) > 1$ for $d_T/\rho \leq 0.1$ [28]. Finally, in general, $[\eta]$ may be expressed as a function of $M$, $R_G$, $R_H$, and a structural function $K_\eta$ that depends on the shape of the solute [33]. Thus, for a monodisperse solute:

$$[\eta] = \pi N_A K_\eta R_G^2 R_H / M \tag{25}$$

where, for example, $K_\eta$ is unity for a rodlike chain or a flexible chain with "free-draining hydrodynamics", and tends to 10/3 for a flexible chain with "non-draining hydrodynamics. For the wormlike chain model, $K_\eta$ may be approximated by the relation [33]

$$K_\eta(L/\rho) = 1 + (7/6)\{1 + \tan h[0.25 \ln(L/340\rho)]\} \tag{26}$$

The preceding relations may be used to estimate the experimental parameters obtained for heterodisperse samples. Thus, for the wormlike chain model [2,29,30]

$$(M_V)_{LS} = \Sigma w_v M_v (1 + 4\delta^2/5)_v = M_w + 4(\delta^2 M_H)_{LS}/5 \tag{27}$$

$$(\delta^2 M_H)_{LS} = \Sigma w_v (\delta^2 M)_v \approx \delta_o^2 M_w (1 + 3L_w/2\rho)^{-1} \tag{28}$$

$$(R_{G,V}^2)_{LS} = (M_V)_{LS}^{-1} \Sigma w_v M_v j(\delta_v)(R_G^2)_v \approx \frac{L_{z+1}L_z}{12} \frac{J(\delta_w)}{(1 + L_{z+1}/4\rho)} \tag{29}$$

$$(R_{G,H}^2)_{LS} = \frac{\Sigma w_v M_v (f_3^2 \delta^2 R_G^2)_v}{\Sigma w_v (\delta^2 M)_v} \approx \frac{L_{z+1}L_z}{12} \frac{(1 + 3L_w/2\rho)}{[1 + (L_{z+1}L_z L_w/4\rho^3)^{2/7}]^{7/2}} \tag{30}$$

$$R_{H,LS} = M_w / \Sigma w_v M_v (R_H^{-1})_v \approx (L_w/2)\{(27L_w/16\rho') + [2(L_w/d_h')^{0.2}]^2\}^{-1/2} \tag{31}$$

where $\rho' = (L_w/L_{(0.5)})\rho$ and $d_h' = (L_w/L_{(-0.2)})d_h$, with $L_{(a)} = (\Sigma w_v L_v^a)^{1/a}$ obtained from the average value of $L^a$ over the molecular weight distribution [34]. For a most probable distribution of $L$, $\rho' \approx 1.09\rho$, $d_h' \approx 1.55 d_h$, and $L_z/L_w = 1.5$, etc.

### Characterization parameters

Owing to the anticipated large value of $\rho$, the effects of intramolecular excluded volume on the chain dimensions are expected to be negligible for *cis*-PBO and small or negligible for *ab*-PBO. Thus, for example, $A_{2,LS}M_w^2/R_{G,LS}^3$ is about one hundred-fold smaller than its limiting value ($\approx 4\pi^{3/2}N_A$) [31], indicating that both $a(L/\rho, d_T/\rho, z)$ and $\alpha_o$ are approximately unity. The strong correlation of $A_{2,LS}$ with the Debye screening length $\kappa^{-1}$ shown in Table 1 for both *cis*-PBO and *ab*-PBO is attributed to the effects of electrostatic interactions on $d_T$, see below. For $a(L/\rho, d_T/\rho, z) \approx 1$, the average over chain lengths simplifies to give $A_{2,LS} \approx A_2$, so that the data on $A_{2,LS}$ give $d_T a(L/\rho, d_T/\rho, z) \approx d_T$ equal to 1.5, 2.5 and 9.2 nm for solutions of *ab*-PBO in MSA, FMSA + 0.1M, and FMSA, respectively. The

data on $A_{2,LS}$ for solutions of *cis*-PBO in MSA, FMSA + 0.1M and FMSA are similar to the values for *ab*-PBO in the corresponding solvents, and give $d_T$ equal to 1.3, 2.1 and 11.1 nm for solutions of *cis*-PBO in MSA, FMSA + 0.1M, or FMSA, respectively.

Analysis of the data on $R_{G,LS}/L_w$ and $R_{H,LS}/L_w$ gives $\rho \approx 18$ nm for the *ab*-PBO in solution in FMSA + 0.1M, assuming a most-probable distribution of chain lengths (i.e., $M_z/M_w = 1.5$, etc.). A value of $\rho \approx 9$ nm has been deduced from the dependence of $[\eta]$ on $M_w$ for solutions of *ab*-PBO in solution in MSA [18]. Use of the estimate $\rho \approx 18$ nm and the preceding relation for $A_2$ gives a calculated expansion factor $\alpha_o \approx 1.03$. Since $\alpha_o$ is essentially unity, the effects of excluded volume may be neglected on the estimate of $\rho$ from data on $R_{G,LS}/L_w$ and $R_{H,LS}/L_w$. The data on $R_{G,LS}/L_w$ give $\rho > 400$ nm for the *ab*-PBO in solution in FMSA, i.e., the chain conformation is rodlike for *ab*-PBO in solution in FMSA, presumably owing to the effects of electrostatic interactions on $\rho$, see below; this estimate of $\rho$ is comparable to $L_w$ for the polymer studied.

As expected if a nearly rodlike chain conformation is conferred by the chain structure, the values of $R_{G,LS}$ and $R_{H,LS}$ do not vary much as a function of the ionic strength of the solvent for *cis*-PBO, despite the wide variation in $d_T$. The values of $\rho$ deduced from the data on $R_{G,LS}$ and the assumed most-probable molecular weight distribution give $\rho \approx 40$ nm. A somewhat smaller estimate of $\rho \approx 25$ nm has been deduced from data on $R_{G,LS}$ over a range of $M_w$ [17]. As noted above, the estimate for $R_{G,LS}$ obtained here is slightly larger than would be interpolated from the data in reference 17 for the same $M_w$. The data on $R_{H,LS}$ are consistent with this estimate if $d_H \approx 1.3$ nm. This is larger than the estimated geometric diameter $d_H \approx 0.5$ nm, and close to the estimate of $d_T \approx 1.3$ nm observed in the solvent with highest ionic strength. This may indicate that $d_H$ reflects the diameter of a solvated segment.

The function $K_{app} = [\eta]M_w/\pi N_A R^2_{G,LS} R_{H,LS}$ is equal to $K_\eta(L/\rho)$ for a monodisperse polymer, and $K_{app} \approx (M_w/M_z)^{1.2}(M_z/M_{z+1})(M_w/M_{(-0.2)})^{0.2} K_\eta(L_w/\rho)$ for a polydisperse linear chain. The data on *ab*-PBO in solution in FMSA + 0.1M give $K_{app} = 0.82$, consistent with the estimate $K_{app} \approx 0.5$ expected for the assumed distribution of molecular weights and $K_\eta(L_w/\rho) \approx 1.5$ corresponding to the relation given above for $K_\eta(L/\rho)$. Similarly, $K_{app}$ is between 0.4 to 0.5 for the solvents used for *cis*-PBO, which is the range expected for the assumed molecular weight distribution if $K_\eta(L_w/\rho) \approx 1$, as expected for a rodlike chain ($L_w/\rho < 1$).

A striking feature of the angular dependence of the scattering on solutions of *cis-ab*-PBO is the substantial difference between $R^2_{G,V} = \{3/[Kc/R_{Vv}(0)]^\circ\}\partial[Kc/R_{Vv}(q)]^\circ/\partial q^2$ and $R^2_{G,H} = \{7/3[Kc/R_{Hv}(0)]^\circ\}\partial[Kc/R_{Hv}(q)]^\circ/\partial q^2$, with $R^2_{G,H} << R^2_{G,V}$, see Figure 2. Using the estimate $\rho \approx 40$ nm given above for *cis*-PBO, together with an assumed most-probable distribution of L, $(R^2_{G,H})_{LS} \approx 0.2 R^2_{G,V}$, consistent with the observed weak angular dependence of $[Kc/R_{Hv}(q)]^\circ$. These parameters give $\delta_o \approx 0.49$ using from the data on $[R_{Hv}(0)/R_{Vv}(0)]^\circ$ for *cis*-PBO, consistent with prior estimates of $\delta_o$ for similar chains [2]. The weaker depolarized scattering for solutions of *ab*-PBO, despite the deduced value of $L_w/\rho < 1$ for solutions in FMSA suggest that $\delta_o$ must be small for this chain, perhaps due to the inclination of the repeat unit axis to the mean axis of the chain in an extended conformation.

### Comparison with theory

For charged chains such as those studied here, both $\rho$ and $d_T$ comprise two terms, one for effects characteristic of the neutral chain (subscript *n*), and one for electrostatic effects (subscript *e*) [5–11]:

$$\rho = \rho_n + \rho_e \tag{32}$$

$$d_T = d_n + d_e \tag{33}$$

The freely-rotating chain model with fixed bond lengths gives $\rho_n \approx 5$ nm for *ab*-PBO. Values of $\rho_n$ have been predicted to be in the range 25 to 80 nm for *cis*-PBO [16,17]. Typically, $0 \leq d_n \leq d_G$, with the lower bound set by the onset of phase separation in the absence of other factors. Presumably, $d_n$ could be negative without phase separation if $d_e$ is large enough, see below.

An electrostatic model based on a charged wormlike cylinder has been developed for both $\rho_e$ and $d_e$ [8–11], and an electrostatic model has been developed for $\rho_e$ for a charged wormlike chain [5–8,12,13]. The former treatment accounts for the formation of ion pairs as $L_c$ approaches $L_B$, and expresses $\kappa d_e$ and $\kappa\rho_e$ in terms of the reduced parameters $\kappa d_G$, $d_G/L_B$ and $L_c/L_B$. Calculations using the model show that for the range of parameters of interest here, $\kappa d_e$ depends only weakly on $d_G$, with $\kappa d_e$ in the range 5 ~ 7, for $d_G = 0.5$ ~ 2 nm, $L_B = 0.9$ nm, and $L_c = 0.5 \cong 1$ nm. Although the trends in $d_T$ observed with ionic strength of the acidic solutions of both *cis*-PBO and *ab*-PBO are consistent with the behavior calculated for $d_e$, the observed $d_T$ are much smaller than the calculated $d_e$. Thus, $d_e/d_T \approx 10$ for solutions in FMSA + 0.1 or MSA, and $d_e/d_T \approx 5$ for solutions in FMSA. This may indicate that $d_n$ is negative, and that solutions of *cis*-PBO or *ab*-PBO would not be soluble in these reagents without the protonation of the macromolecule. Indeed, both polymers come out of solution on addition of small amounts of water, which acts as a stronger base than the polymer, leading to deprotonation and precipitation.

The results of electrostatic models may be expressed in the form

$$\rho_e \approx \{d_G/L_B\}k_e(d_G\kappa, L_B/L_C)g_e(L\kappa)\kappa^{-1} \tag{34}$$

For the wormlike chain model (and a univalent electrolyte), $k_e(d_G\kappa, L_B/L_C) = (4d_G\kappa)^{-1}(L_B/L_C)^m$, with m = 2 for $L_B/L_C < 1$, and zero otherwise, and $g_e(L\kappa) \sim (1 + 18/(L\kappa)^2)^{-1}$ (an exact from is available) [6,7]. Thus, $\rho)_e = g_e(L\kappa)/(4L_B\kappa^2)$ with this model for $L_B/L_C > 1$. The model is expected to apply only in the range $\rho_e < \rho_n$. The function $g_e(L\kappa)$ is set to unity with the developments for the wormlike cylinder model [9–11], and for the range of parameters of interest, the dependence of $k_e(d_G\kappa, L_B/L_C)$ on $d_G\kappa$ is weaker with the charged wormlike cylinder model than for the chain model, with $k_e(d_G\kappa, L_B/L_C)$ equal to 1 and 2 for solutions in MSA (or FMSA + 0.1M) and FMSA, respectively. This gives $\rho \sim 5 + 1 = 6$ nm for *ab*-PBO in solution in FMSA + 0.1M using the estimate $d_G/L_B = 0.56$ and $\kappa$ from Table I, in comparison with the value $\rho \sim 18$ nm given above. Correspondence between the calculated and measure values would require an unexpectedly large value for $d_G$, or a substantial decrease in the estimate for $L_c$. Similarly, the estimate of $\rho \sim 400$ nm obtained for *ab*-PBO in solution in FMSA is substantially larger than the calculated $\rho_e \sim 25$ nm obtained with the model. The relative independence of $\rho$ from $\kappa$ for solutions of *cis*-PBO indicates that $\rho_e < \rho_n$ for this chain.

The large value of $\rho$ for *ab*-PBO in solution in FMSA may be surprising in comparison with the much smaller estimate found for *cis*-PBO, despite the larger value of $\rho_n$ for *cis*-PBO. An explanation for this behavior may reside in the constraints to further chain extension for *cis*-PBO owing to its structure. By contast, the rotational freedom in *ab*-PBO permits considerable extension of the chain relative to the conformation of the neutral chain.

The electrostatic interactions are thus not able to effect further extension of the *cis*-PBO chain, whereas they appear to stabilize an extended zig-zag conformation *ab*-PBO chain in solution in FMSA, so as to minimize the electrostatic interactions among the protonated repeat units (the Debye screening length far exceeds the charge separation in this case). The electrostatic model for the charged wormlike cylinder does not appear to account for this behavior.

## CONCLUSIONS

The data on *cis*-PBO and *ab*-PBO reveal the effects of electrostatic interactions among the protonated chains through a thermodynamic segment diameter $d_T$ that depends markedly on the Debye electrostatic screening length $\kappa^{-1}$. The analysis suggests that the electrostatic component $d_e$ must be large enough to offset a neutral component $d_n$ in $d_T$, providing the mechanism for dissolution of the charged chains. The data give a persistence length $\rho \approx 40$ nm for *cis*-PBO, essentially independent of $\kappa^{-1}$. Thus, for this chain the electrostatic component $\rho_e$ to $\rho$ must be small in comparison with the neutral component $\rho_n$ to $\rho$. This appears to be in reasonable accord with estimates of $\rho_n$ based on conformational analyses, and $\rho_e$ using an electrostatic model. By contrast, $\rho$ is found to depend markedly on $\kappa^{-1}$ for *ab*-PBO, with $\rho$ much larger than $\rho_n$ for all of the systems studied. The observed $\kappa\rho$ vary from 20 to 50 with $\kappa^{-1}$ increasing from 0.8 to 8 nm for *ab*-PBO. Thus, *ab*-PBO may be considered to be a charged wormlike semiflexible chain in solvents with low $\kappa^{-1}$ (high ionic strength), and rodlike in solvents with larger $\kappa^{-1}$. By comparison, values of $\kappa\rho$ calculated with an electrostatic model for a charged wormlike cylinder are about ten-fold smaller. The discrepancy is attributed to the failure of the electrostatic model to account for the discrete rotational states available to the *ab*-PBO chain.



### Acknowledgments

This study comprises a portion of the Ph.D. dissertation of VJS. Partial support of VJS by a grant from the Air Force Materials Laboratory, and of GCB by the Polymers Program, National Science Foundation is gratefully acknowledged.

### References

1. G. C. Berry, and P. R. Eisaman, *J. Polym. Sci. Polym. Phys. Ed.*, **12**, 2253 (1974).
2. C. Lee, S.-G. Chu, and G. C. Berry, *J. Polym. Sci. Polym. Phys. Ed.*, **21**, 1 (1983).
3. C.-P. Wong, H. Ohnuma, and G. C. Berry, *J. Polym. Sci.: Polym. Symp.*, **65**, 173 (1978).
4. D.B. Roitman, M. McAdon, J. McAlister, E. Martin, and R. A. Wrestling, *J. Polym. Sci., Part B: Polym. Phys.*, **32**, 1157 (1994).
5. J. Skolnick, and M. Fixman, *Macromolecules*, **10**, 944 (1977).
6. T. Odijk, *J. Polym. Sci. Polym. Phys. Ed.*, **15**, 477 (1977).
7. T. Odijk, and A. C. Houwaart, *J. Polym. Sci. Polym. Phys. Ed.*, **16**, 627 (1978).
8. M. Fixman, and J. Skolnick, *Macromolecules*, **11**, 863 (1978).
9. M. L. Bret, *J. Chem. Phys.*, **76**, 6243 (1982).
10. M. Fixman, *J. Chem. Phys.*, **76**, 6346 (1982).
11. R. M. Davis, and W. B. Russel, *J. Polym. Sci. Polym. Phys. Ed.*, **24**, 511 (1986).
12. M. Schmidt, *Macromolecules*, **24**, 5361 (1991).

13. S. Förster, M. Schmidt, and M. Antonietti, *J. Phys. Chem.* **96**, 4008 (1992).
14. P. Metzger Cotts, and G. C. Berry, *J. Polym. Sci., Polym. Phys. Ed.*, **21**, 1255 (1983).
15. W. J. Welsh, and J. E. Mark, *Polym. Bull.*, **8**, 721 (1982).
16. R. Zhang, and W.L. Mattice, *Macromolecules*, **25**, 2937 (1992).
17. D. B. Roitman, R. A. Wessling, and J. McAlister, *Macromolecules*, **26**, 5174. (1993).
18. A. W. Chow, S. P. Bitler, P. E. Penwell, D. J. Osborne, and J. F. Wolfe, *Macromolecules*, **22**, 3514 (1989).
19. G. C. Berry, in *Contemporary Topics in Polymer Science*, E. M. Pearce, J.R. Schaefgen, Eds, Plenum Press, New York, 1977, p. 55.
20. D. B. Roitman, private communication.
21. R. J. Gillespie, and E. A. Robinson, in *Non-Aqueous Solvents*, T. C. Waddington Ed., Academic Press, New York, 1965, Chapt. 4.
22. H. Yamakawa, *Modern Theory of Polymer Solutions*, Harper and Row, New York, 1971.
23. G. C. Berry, *J. Polym. Sci.: Polym. Symp.*, **65**, 143 (1978).
24. G. C. Berry, in *Encyclopedia of Polymer Science and Engineering*, Vol. 8, H. Mark *et al.* Ed., John Wiley and Sons, Inc., 1987, p. 721.
25. G. C. Berry, *Adv. Polymer Sci.*, **114**, 233 (1994).
26. H. Benoit, and W.H. Stockmayer, *J. Phys. Radiumn*, **17**, 121 (1956).
27. B. J. Berne, and R. Pecora, *Dynamic Light Scattering*, John Wiley and Sons, Inc. (1976)
28. H. Yamakawa, and W. Stockmayer, *J. Chem. Phys.*, **57**, 2843 (1972).
29. R. Furukawa, and G. C. Berry, *Pure Appl. Chem.*, **57**, 913 (1985).
30. C. Wei-Berk, and G. C. Berry, *J. Polym. Sci., Part B: Polym. Phys.*, **28**, 1873 (1990).
31. E. F. Cassasa, and G. C. Berry, in *Comprehensive Polymer Science*, Vol. 2, G. Allen Ed., Pergamon Press, New York, 1988, Chapt. 3.
32. M. Muthukumar, B. G. Nickel, *J. Chem. Phys.*, **86**, 460 (1987).
33. G. C. Berry, *J. Polym. Sci., Part B: Polym. Phys.*, **26**, 1137 (1988).
34. G. C. Berry, in *Encyclopedia of Materials Science and Engineering*, M. B. Bever Ed., Pergamon Press, Oxford, 1986, p. 3759.